Performance of the Aerobell Extendible Rocket Nozzle

G. A. HOSACK* AND R. R. STROMSTA†
Rocketdyne, A Division of North American Rockwell, Canoga Park, Calif.

Extendible nozzles are currently being considered for space propulsion. The aerobell is one promising configuration for this application. The nozzle extension is a translating shroud cooled by the engine turbine exhaust gases. The turbine exhaust is introduced subsonically into a step discontinuity at the basic nozzle extension interface and separates the primary stream and the extension walls. Results of an extensive theoretical and experimental program for the design and performance analysis of aerobell engines are discussed. The theory is compared with data taken from cold-flow and simulated hot-flow test results. The results indicate that the aerobell provides performance gains on the order of 2% relative to the basic nozzle. The performance trends and magnitudes are shown to be predictable (within 0.3%) using the methods developed.

Nomenclature

A	=	area
C_F	=	nozzle thrust coefficients, F/P_cA^*
c^*	=	characteristic velocity, $P_cA^*g_c/\dot{w}$
D	=	diameter
F	=	thrust
g_c	=	gravitational units conversion factor
L	=	nozzle axial length
P	=	pressure
R	=	radius
T	=	temperature
$\dot{w}$	=	flow rate, lbm/sec
X	=	axial length
γ	=	ratio of specific heats
ϵ	=	area ratio, area/throat area

Superscript

*	=	sonic conditions

Subscripts

a, B, c, o	=	ambient, base, chamber, and stagnation conditions, respectively
p, s	=	primary and secondary conditions, respectively
SH, t, w	=	shroud, throat, and wall conditions, respectively

Introduction

VARIOUS types of extendible nozzles are being considered for propulsion systems for length-limited envelopes in upper stage vehicles. The aerobell concept furnishes one promising configuration (Fig. 1). The translating shroud is cooled by the engine turbine exhaust gases introduced subsonically through the gap between the basic nozzle and the extension walls. The interaction of the primary flow with the turbine exhaust gases provides a complex flowfield that must be analyzed to determine the over-all engine performance and cooling requirements.

In this paper, the results of an extensive experimental and theoretical program for the design and performance analysis of aerobell engines are discussed. The theory developed is based on the base flow model of Korst.[1] Modifications developed by several other researchers[2–6] in addition to those discussed herein have been included in the theory.

Presented as Paper 69-4 at the 7th AIAA Aerospace Sciences Meeting, New York, January 20–22, 1969; submitted February 13, 1969; revision received August 13, 1969. This work was supported by NASA Contract NAS8-19.

* Principal Scientist, Heat and Fluid Physics Group, Research Division. Member AIAA.

† Member of the Technical Staff, Aerothermodynamics Unit, Advanced Projects. Member AIAA.

Cold-Flow Experimental Program

A cold-flow nozzle test program was conducted. The models (Fig. 2) were $\frac{1}{16}$-scale replicas of full-scale J-2 hardware. The porous plates were made of uniformly perforated steel sheets; nominal effective porosities were 7.8% for the conical aerobell and 3.1% for the cylindrical aerobell, respectively. The lower porosity material was used with the cylindrical aerobell to compensate for its larger base area since it was desired to keep the net effective secondary flow area similar for the conical and cylindrical aerobell extensions. The cylindrical aerobell extension was made in two sections to provide for a "long" and a "short" extension. The short one was the same length as the conical aerobell. In both aerobells, the secondary flow was introduced into a secondary manifold through four tubes spaced 90° apart. Each tube in turn was divided by a tee to provide a total of eight secondary inlet ports to insure uniform circumferential secondary flow distribution. The porous plate flow area was chosen to provide local choking of the secondary flow as it passed through the small holes to further insure uniform flow conditions under all test conditions. Geometries are summarized in Table 1. All of the models were machined from corrosion resistant stainless steel.

Static and total pressure taps were provided to record local wall and stagnation pressures. A windshield was used to protect the force balance from possible recirculation effects. Sonic venturi flow meters were used to measure weight flow rates. Resistance-type temperature sensors (Rosemount) used in conjunction with a self-balancing potentiometer were used to record temperature.

The Rocketdyne Rocket Nozzle Test Facility is essentially a blowdown, downdraft-type internal wind tunnel. Dried and filtered compressed air, usually near normal atmospheric temperature (T_o = 50 ± 20°F), is expanded through the nozzle to a controlled ambient pressure (simulated altitude) maintained by high-capacity vacuum pumps. The models were individually mounted on an axial-component force measuring device (single-component force balance) that incorporated a load cell as the sensing element. All program testing was performed without a diffuser to minimize diffuser feedback at low pressure ratios.

Air was used in the primary and secondary streams for the majority of the testing, but CF_4 was also used for testing the conical aerobell to provide data to assist in the scaling of

data to hot-firing conditions. The shifting specific heat ratio γ of CF_4 closely approximates that of actual hot-firing combustion products when undergoing expansion within the nozzle. It is a heavy nonreactive gas (molecular weight = 88) with a γ that varies with pressure and temperature. It is not an ideal gas. Based on DuPont Co. data concerning the physical and thermodynamic properties of CF_4, a digital computer program was developed to generate the gasdynamic expansion properties in a tabular form suitable for use in currently available method-of-characteristics nozzle analysis and design programs.

Thrust Coefficients

The vacuum thrust coefficient is defined as

$$C_{F(\text{vac})} = F_{(\text{vac})}/P_cA_p^* = F_{(\text{vac})} \cdot g_c/\dot{w}_pc_p^* \quad (1)$$

For a system that utilizes secondary flow, the definition can be extended to

$$C_{F(\text{vac})} = F_{(\text{vac})} \cdot g_c/(\dot{w}_pc_p^* + \dot{w}_sc_s^*) \quad (2)$$

For an extendible nozzle, the incremental nozzle extension thrust coefficient ΔC_F, is defined as

$$\Delta C_{F(\text{vac})} = \Delta F/P_cA_p^* \quad (3)$$

where ΔF is the difference in vacuum thrusts. The use of $\Delta C_{F(\text{vac})}$ in the results to follow refers to $\Delta F/P_cA_p^*$ only, Eq. (3), not Eq. (2), even for cases where secondary flow was used.

Results of Cold-Flow Test Program

The basic J-2D bell nozzle was tested at high-pressure-ratio conditions to determine the vacuum thrust performance; seven runs were made using air at P_c = 100 psia, and two runs were made using CF_4 at P_c = 40 psia. The nozzle had a smooth wall contour, and no secondary flow was used. The average vacuum thrust coefficients for the two sets of test conditions were 1.660 and 1.792, respectively. Typical schlieren photographs of the exhaust plumes are shown in Figs. 3a and 3b. Note that the shock structure in the center portions of the plume is longer for air.

Table 1 Extendible nozzle cold-flow model geometric parameters

Item	Basic nozzle	Extensions: Conical aerobell	Extensions: Cylindrical aerobell
Scale factor (model/full)	0.0602	0.0602	0.0602
Geometrical throat diameter D_t, in.	0.8870	0.8870	0.8870
Model contour exit diameter D_e, in.	4.622	6.571	6.571
Model contour area ratio $\epsilon = (A_e/A_t)$	27.16	54.88	54.88
Model contour length from throat L_e, in.	5.284	9.086	9.179 (12.80)[a]
Dimensionless contour length, L_e/R_t	11.91	20.49	20.70 (28.86)[a]
Percent length relative to 15° cone, %	75.7	85.7	86.6 (120.7)[a]
Extension divergence half-angle, deg	...	6.60	...
Secondary flow configurations	None	Porous plate	Porous plate
Location of secondary injector, X/R_t	...	11.95	12.09
Base area ratio $\epsilon_B = (A_B/A_t)$	...	12.78	26.17
Extension wall area ratio $\epsilon_w = (A_w/A_t)$	...	13.47	...
Average effective secondary flow A_s^*, in.^{2}	...	0.62	0.50

[a] Long aerobell.

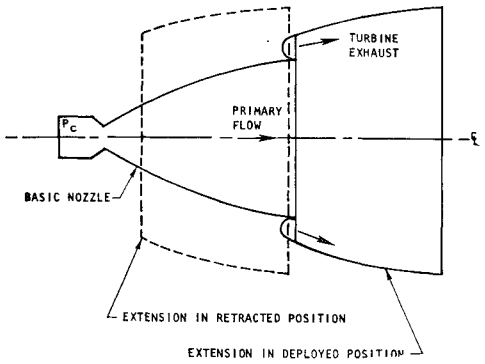

Fig. 1 Aerobell concept.

The basic J-2D fitted with the 6.6° conical extension was tested at high-pressure-ratio conditions; 17 tests were performed at P_c = 100 psia using air in both the primary and secondary streams. Nine tests were performed using CF_4 at P_c = 40 psia in the primary stream with air in the secondary stream. Small amounts of secondary flow substantially increased over-all nozzle thrust performance (Fig. 4). Larger amounts, however, caused the net vacuum performance to reach a maximum and then decrease as more secondary flow was added. The point of maximum net nozzle performance occurred at different weight flow ratios for air/air and CF_4/air. For the CF_4/air tests, the average c_s^*/c_p^* ratio was 1.651 because of the high molecular weight of CF_4 relative to air. Typical schlieren photographs of nozzle plumes for air and CF_4 with 0 and 2% secondary flow are shown in Fig. 3.

Two 55:1 area ratio cylindrical aerobell nozzle configurations were tested with air/air. Ten tests each were performed on the long and short cylindrical aerobell configurations using $\dot{w}_s/\dot{w}_p$ from 0 to 3%. Performance trends with secondary flow for the two configurations are plotted in Fig. 4. Schlieren photographs are shown in Fig. 3.

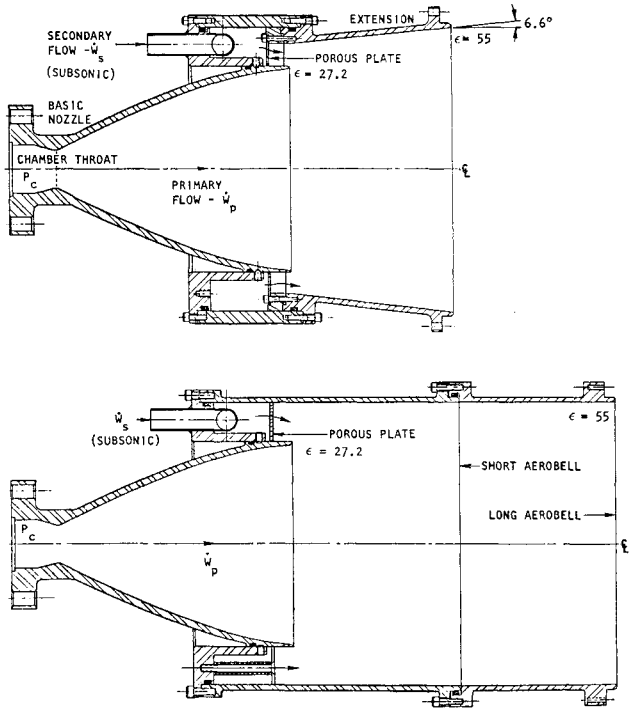

Fig. 2 Cold-flow test models.

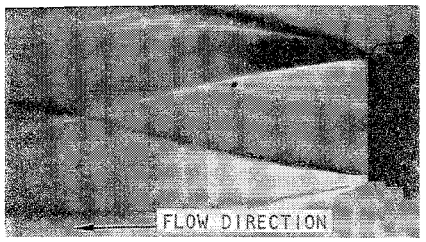

a) $P_c/P_a = 1100$, $\dot{w}_s/\dot{w}_p = 0$, $\epsilon = 27.2$ basic nozzle using air

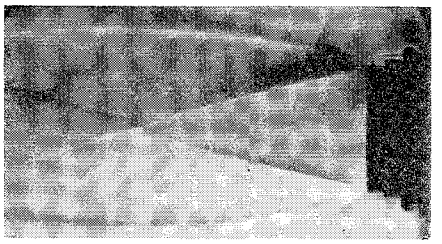

b) $P_c/P_a = 974$, $\dot{w}_s/\dot{w}_p = 0$, $\epsilon = 27.2$ basic nozzle using CF_4

c) $P_c/P_a = 1177$, $\dot{w}_s/\dot{w}_p = 0$, $\epsilon = 55$ conical aerobell using air/air

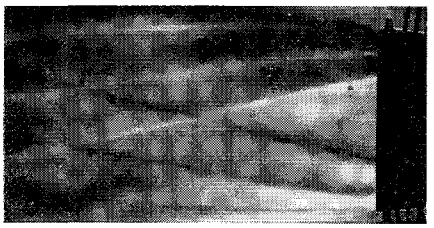

d) $P_c/P_a = 1232$, $\dot{w}_s/\dot{w}_p = 1.97\%$, $\epsilon = 55$ conical aerobell using air/air

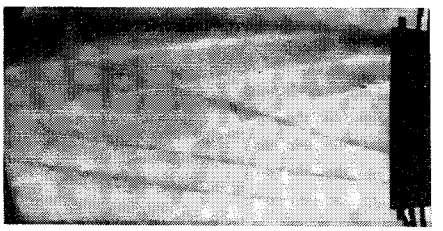

e) $P_c/P_a = 788$, $\dot{w}_s/\dot{w}_p = 2.03\%$, $\epsilon = 55$ conical aerobell using CF_4 air

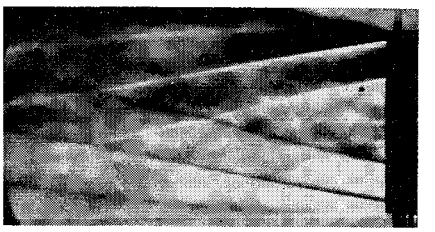

f) $P_c/P_a = 1228$, $\dot{w}_s/\dot{w}_p = 2.80\%$, $\epsilon = 55$ short cylindrical aerobell using air/air

Fig. 3 Schlieren photographs of nozzle exhaust plumes.

Analysis

For the purpose of analysis, the theory is conveniently divided into two regimes: small-bleed and large-bleed. In the former regime, the flow near the base is characterized by a recirculating pattern; whereas, in the latter regime the bleed rate is sufficient to suppress the reverse-flow component and no reverse flow exists (Fig. 5).

Small-Bleed Theory

The analytical model for the small-bleed case is based on the assumption that reverse flow occurs in the base region. The bleed rate is not large enough to suppress the reverse-flow portion (Fig. 5). It is assumed that a supersonic primary stream expands isentropically into a lower-pressure base region. The static pressure is assumed to be constant in the base region downstream to the point where the recompression region is reached. At this point, the inviscid flow is turned parallel to the shroud contour with an accompanying pressure rise. This pressure gradient is imposed on the turbulent shear layer, causing deceleration and, for the slower elements, a reversal of flow back into the base region. The discriminating streamline just stagnates in the adverse pressure gradient. All higher-velocity elements penetrate the recompression region and escape into the downstream flowfield; all those possessing lower velocity are turned back (Fig. 6).

On the basis of simplified shear layer equations, an error-function similarity velocity profile is obtained. This velocity profile is superimposed on the corresponding inviscid jet boundary (that boundary which would exist in the absence of a viscous shear layer) to describe the shear layer.

The effect of the initial boundary layer of the primary flow, resulting from the boundary-layer build-up inside the primary nozzle, is accounted for by the "virtual origin" method. It is assumed that a virtual origin of mixing is located upstream of the secondary inlet, a small distance, and thereby approximates the effect of the initial boundary layer through the use of an equivalent shear layer (Fig. 7).

Based on the foregoing assumptions, the point on the free-jet boundary at which recompression begins can be determined. It corresponds to the unique point at which the flow

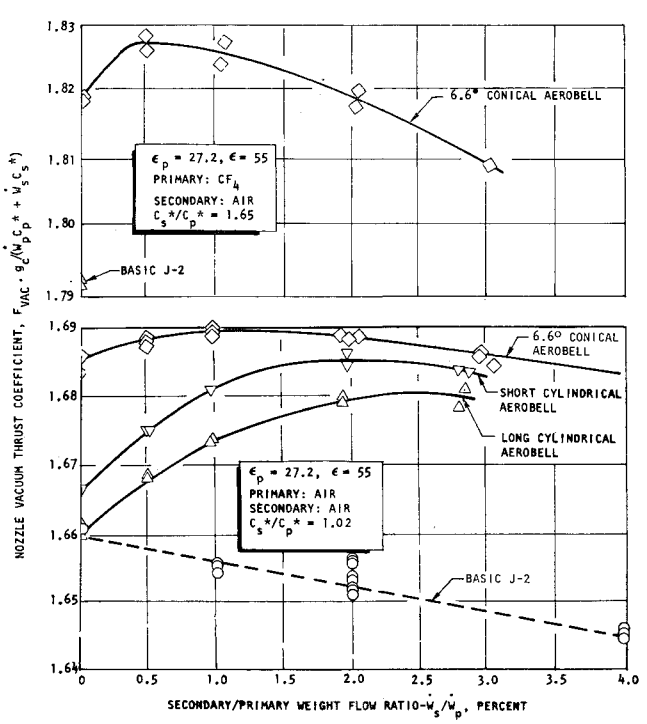

Fig. 4 Nozzle vacuum thrust performance vs secondary flowrate cold-flow experimental data.

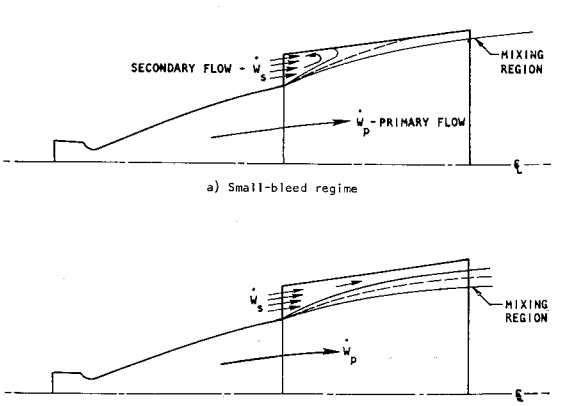

Fig. 5 Aerobell base bleed models.

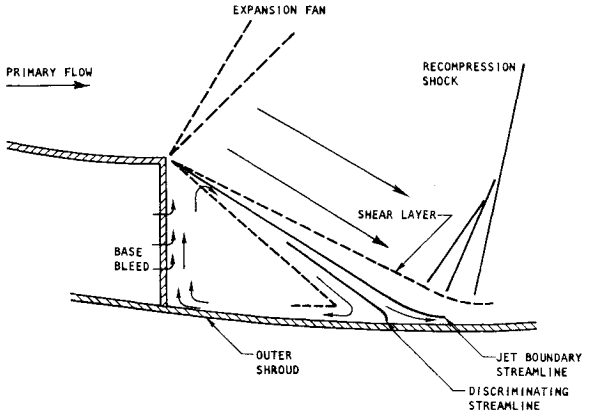

Fig. 6 Small-bleed aerobell.

area of the recirculating stream is compatible with the zero point on the velocity profile as determined by conservation principles (Fig. 8).

The velocity profile at this point is chosen to have the shape indicated in Fig. 8. The lower portion or "tail" of the forward-moving error-function velocity profile is distorted by viscous forces resulting from the reverse flow. It is assumed that the upper portion of the velocity profile for the forward-moving flow retains the error-function form, but that the lower portion assumes the shape of the tangent to the original profile at the point of inflection as indicated in Fig. 8.

This method for determining the base pressure is essentially the Korst base flow model[1] incorporating the virtual origin method of Kirk,[2] the velocity profile at the start of recompression as shown in Fig. 8 and a recompression factor N as a function of Crocco number based on experimental data. The recompression factor is defined in the manner presented by Nash.[3]

The computational procedure involves assuming a base pressure and calculating the bleed necessary to obtain this base pressure. A base pressure vs bleed curve can then be obtained. For any desired bleed-rate ratio, the base pressure can be determined from the curve. The computation scheme is as follows.

For a given nozzle geometry, the primary flowfield is calculated by the method of characteristics up to the last right-running characteristic line from the nozzle exit (Fig. 9, line AB). A boundary-layer and drag analysis for the primary nozzle is also performed using standard calculation procedures. These calculations determine the primary nozzle performance. A method-of-characteristics plume program is then used to generate constant-pressure, inviscid plume boundaries for various assumed values of base pressure. The base pressure computer program as previously outlined

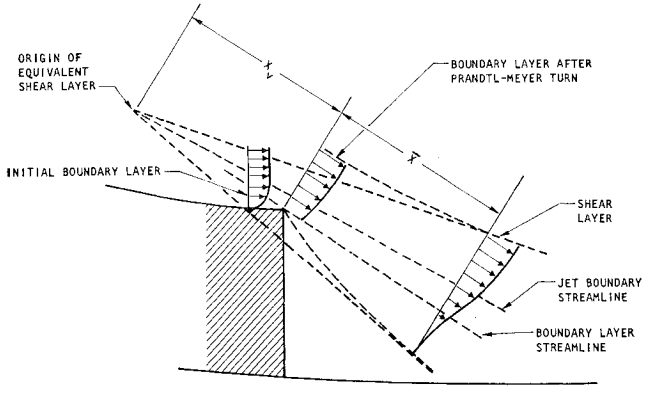

Fig. 7 Virtual origin method for initial boundary layer.

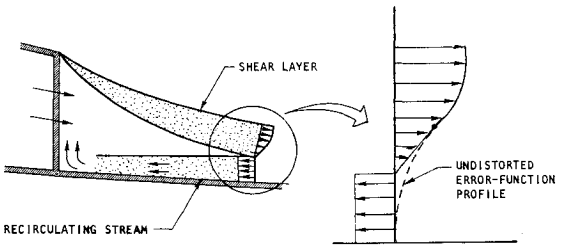

Fig. 8 Location of start of recompression.

is next used to determine the secondary flow rate necessary to produce the assumed values of base pressure.

For cylindrical aerobells, the total performance is obtained by adding the primary thrust to the base thrust obtained by multiplying the base pressure for the desired bleed by the base area. The drag along the outer shroud can be estimated and subtracted out to obtain the over-all thrust of the system.

It should be emphasized that the base pressure computed by this scheme is the so-called "effective base pressure" and is defined as that pressure which when multiplied by the base area produces the base thrust. In actuality, the wind-tunnel tests utilized a porous plate through which the secondary flow was supplied in a choked condition. Therefore, the total base thrust is comprised of the actual integrated pressure force on the plate plus the contribution from the momentum of the secondary flow issuing through the pores.

The over-all thrust calculation for the conical aerobell in the small-bleed regime is very difficult since little is known on predicting the details of the flow through the recompression region. This is necessary to obtain the integrated thrust along the outer shroud contour. It was postulated that the flowfield through the compression shock could be calculated using an exact shock method-of-characteristics computer program. However, this investigation was not performed because of greater interest in the large-bleed performance calculations.

Large-Bleed Theory

It is assumed that if the bleed rate is large, the base pressure becomes large enough that the annular region "pops open" and all of the secondary flow escapes through this region. Figure 10 displays the assumed inviscid flowfield for the large-bleed regime. The primary flow is delivered along the centerline of the nozzle with the secondary flow entering in an annulus about the primary. The primary flow expands from the nozzle exit pressure to the secondary entrance pressure through a Prandtl-Meyer expansion fan. Expansion waves from opposite corners of the primary nozzle intercept the jet boundary and cause it to curve concave toward the axis as shown in Fig. 10.

The shape of the jet boundary allows the subsonic secondary flow to choke at the minimum area, provided that the secondary entrance Mach number and pressure are high

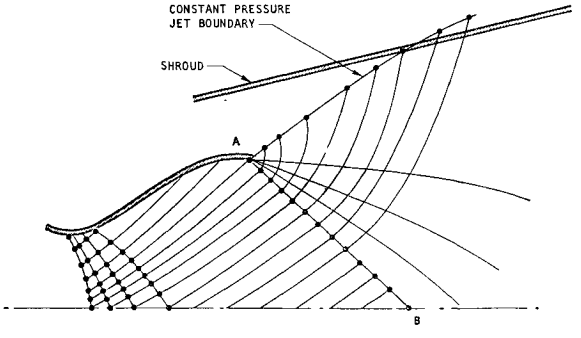

Fig. 9 Primary nozzle flowfield.

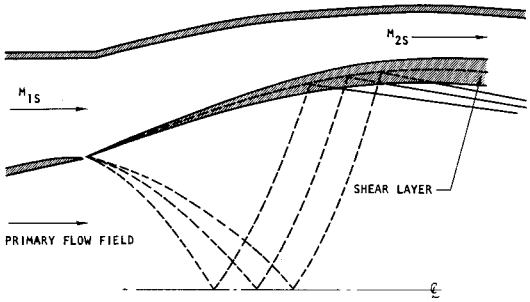

Fig. 10 Large-bleed aerobell.

enough to prevent the jet boundary from intercepting the wall before reaching minimum area for the secondary flow. The basic physical requirement for this flowfield is that the pressure across the boundary of the primary and secondary streams be continuous.

It has been found that a stable solution for the secondary stagnation pressure as a function of secondary flow rate is guaranteed by choking the secondary stream at its minimum area. It is assumed that mixing between the primary and secondary streams does not appreciably affect the inviscid flowfield, and that the effects of mixing can be accounted for by superimposing the mixing region on the inviscid solution by satisfying the momentum relations for the shear flow.

The calculation procedure for the large-bleed regime employs the method of characteristics to determine the primary flowfield by matching the pressure along the inviscid jet boundary with that predicted by a one-dimensional variation of the secondary flowfield properties. This method is essentially the same as that presented by Addy[4] for calculating ejector operating characteristics. For a given static pressure at the base exit plane, a secondary stream Mach number is assumed and the flowfield is computed to the choking location or minimum area, whichever is reached first. The secondary stream Mach number is then iterated until choking occurs at minimum area. This Mach number gives the solution.

The associated bleed rate can then be determined for hot or cold flow. The mixing effects, which are assumed to be of second order, are then estimated and superimposed on the inviscid solution to obtain the corrected secondary bleed rate. A constant-pressure mixing analysis similar to that of

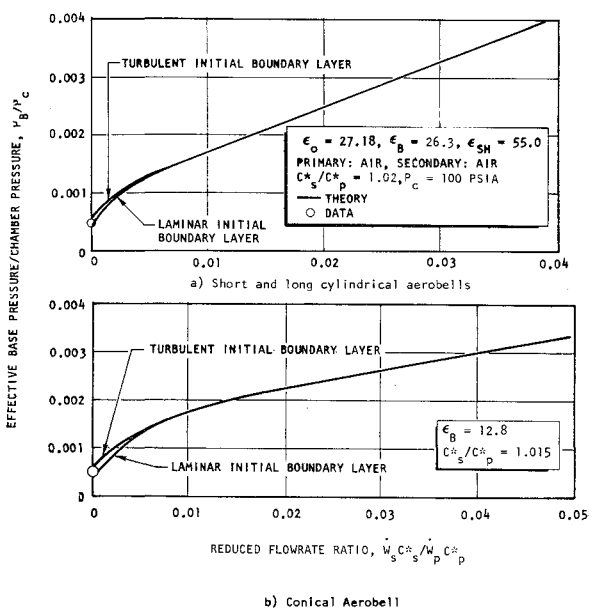

Fig. 11 Effective base pressures.

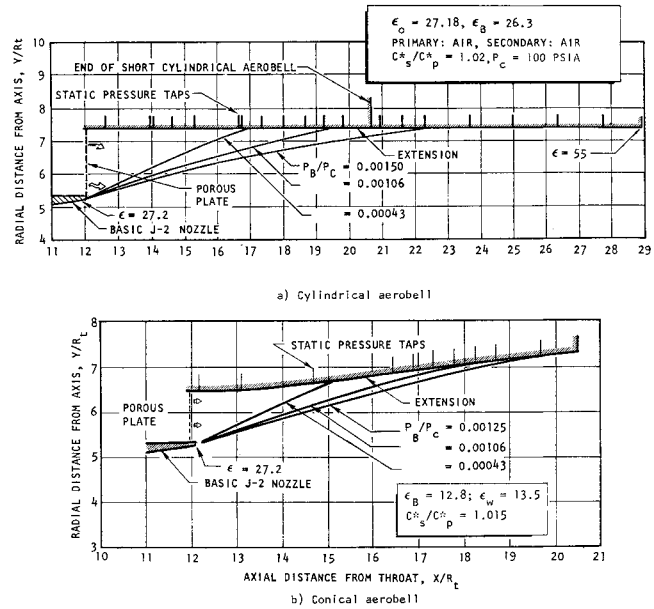

Fig. 12 Constant-pressure, inviscid jet boundaries.

Korst[5] is used to approximate the mixing up to the choking location.

The flow downstream of the choking point is calculated in the same manner as described above for the flow upstream of the choking point. The thrust developed by the secondary flow is then calculated by integrating the pressure along the shroud contour and adding the base thrust.

The previous discussion is based upon the condition that the flow chokes at minimum area inside the shroud contour. For short contours, the previous condition cannot be met, and it is assumed that the flow chokes at the exit plane.

The computation scheme for determining the performance of the large-bleed aerobell is as follows.

The primary nozzle performance is calculated in the same manner as for the small-bleed case. The large-bleed performance program as previously outlined is next used to calculate the secondary performance contributions and uncorrected secondary flow-rate ratios for assumed values of static pressure at the base. The mixing corrections are then calculated using methods similar to those developed by Korst and Chow.[5] The drag of the secondary flow along the extension wall is calculated using the secondary flow properties and the predicted pressure profile for the inviscid solution. The displacement thickness is also calculated for the wall boundary layer so that it can be used, in addition to the mixing correction, to compute the corrected secondary flow rate for the assumed static pressure at the base.

It should be emphasized that in the large-bleed theory, the assumption has been made that mixing effects can be calculated after the inviscid solution has been obtained and the results can be superimposed. For large flow rates ($\dot{w}_s/\dot{w}_p$ perhaps on the order of 10 to 20%), the shear layer thickness is small compared to the remaining flow of secondary flow passing through the choking point and the assumption appears reasonable. However, for lower flow rates (perhaps 2 to 3%, but still considered in the large-bleed regime), the shear layer may actually spread to the wall. For this case, the thickness of the shear layer is relatively large and no annulus of pure secondary flow passes through the choking region. A complex variable pressure mixing program is required for the analysis. Also, the choking phenomenon becomes more complex in that choking for mixed flow has to this date not been completely understood. Nevertheless, the large-bleed theory is still applied to this case in the hope that the analytic treatment, even though approximate for

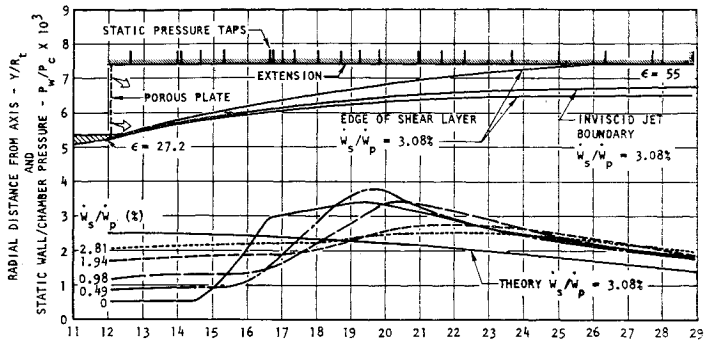

Fig. 13a Long cylindrical aerobell

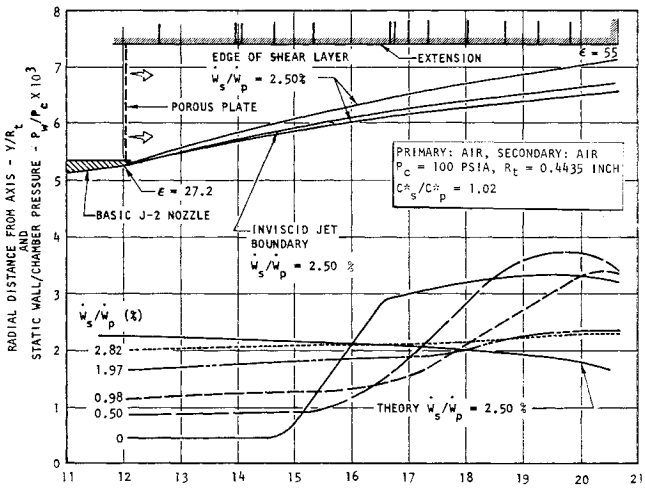

Fig. 13b Short cylindrical aerobell

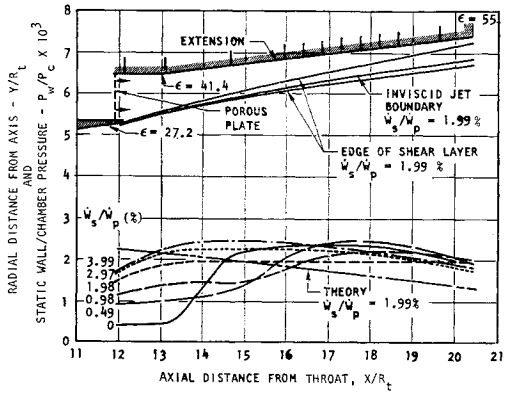

Fig. 13c Conical aerobell

Fig. 13 Large-bleed, variable-pressure jet boundaries, shear layers, and pressure profiles.

the reasons given previously, may provide the proper trends and guidelines for aerobell design and analysis.

Comparison of Theory and Experiment

Base Pressure Calculations

The calculated effective base pressures of the wind-tunnel models are shown plotted in Figs. 11a and 11b. Calculations for the assumptions of both laminar and turbulent initial boundary layers (from the primary nozzle) are shown. The experimentally determined base pressures for zero bleed are also indicated in Figs. 11a and 11b. For cases with bleed, the effective base pressure for the models tested is the result of the impulse of the flow through the porous base plate plus the pressure force acting on the base plate between the pores. Since no pressure measurements were taken between the pores, it is difficult to ascertain the experimental values for the effective base pressure when the bleed rate is nonzero. The effective base pressures for the short and long cylindrical aerobells were equal for the chosen configurations.

To generate these base pressure curves, the small-bleed theory was used to predict the effective base pressure up to base-bleed flow rates large enough that the bleed fills the shear layer. The large-bleed theory was used from higher flow rates down to base-bleed flow rates small enough to cause the effective Mach number at the base plane to be less than 0.1. The intermediate, or transition range, for the base pressure curve was determined by a smooth curve joining the small- and large-bleed solutions.

Jet Boundary Calculations

Several constant pressure inviscid jet boundaries were calculated for the models tested (Fig. 12). These boundaries were assumed to exist at constant pressure (up to the point at which recompression begins) and were used as input to the small-bleed base pressure program.

The inviscid variable-pressure jet boundaries and associated shear layers as calculated by the large bleed theory for particular flow rate ratios are shown in Fig. 13. Also shown in Fig. 13 are predicted and experimentally measured wall pressure profiles. Note that the bleed flow rate ratios do not exactly coincide with any particular test values. Since the large-bleed theory determines the bleed for an assumed static pressure at the base, an iteration is necessary to obtain results for any given flow rate ratio desired.

Also note that the theoretical and experimental wall pressure profiles do not agree. This is because of the porous plate effect (secondary flow introduced and choked flow through the pores). However, it will be seen later that the integrated thrusts resulting from these pressure distributions do agree with test data.

Figure 13 indicates that the size of the shear layer is not small compared with the inviscid core of secondary flow which escapes. In fact, Fig. 13a indicates that the shear layer strikes the wall so that no annulus of inviscid secondary flow escapes. It was found, however, that the large-bleed theory remains valid down to bleed flow rates small enough that the shear layer intersects the wall. This result is somewhat surprising in that the theory considers the shear layer effect as second order, and this is not the case at the lower end of the large-bleed flow regime.

Performance Calculations

The theoretical and experimental performance values for the aerobells tested are shown in Figs. 14 and 15: the inviscid curve, the mixing-only curve (no drag corrections), and the net curve including mixing and drag. The performance is plotted as a function of the reduced flow rate ratio $\dot{w}_s c_s^*/\dot{w}_p c_p^*$. This quantity is used to account for property differences between the primary and secondary streams and allows scaling when secondary properties change. For example, Fig. 15 is applicable for various values of c_s^* (varying T_{os} and/or gas constant). The use of the reduced flow rate ratio is very similar to that of the corrected dimensionless bleed parameter used in Refs. 1 and 6.

For the calculations, the large-bleed theory was extended down to base flow rates small enough that the shear layer intersected the wall. The drag calculations for the large-bleed regime were made using the assumption that secondary flow properties prevail in the flow along the wall as the boundary layer grows. The calculated displacement thickness was then used to correct the base bleed flow rate. The

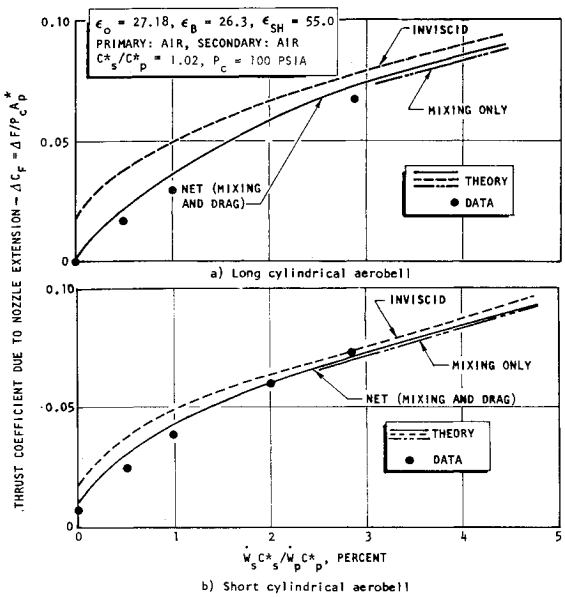

Fig. 14 Cylindrical aerobell shroud thrust contributions.

drag, itself, was found to be very small since a low stagnation-pressure flow exists along the wall.

For the small-bleed portions of these plots, the drag was calculated in an approximate fashion. It was assumed that the primary flow exists along the wall and that the wall pressure is constant and equal to the average of the base pressure and the pressure after the flow has turned parallel to the shroud as predicted by the small-bleed theory. Then, only the drag contribution for the flow downstream of the predicted point at which the recompression begins was used. It was also assumed that the zero-bleed drag was a good approximation for all cases in the small-bleed regime. This assumption is based on the observation that as the bleed rate increases, so does the level of the base pressure. This is compensated by the fact that the recompression point moves farther downstream along the wall and, therefore, results in a shorter effective drag length downstream of the recompression station.

For the conical aerobell, the wall thrust must be calculated to obtain the total performance prediction. For the small-bleed regime it is very difficult to predict the wall pressure profile downstream of the recompression zone. However, the wall thrust can be estimated by the following procedure which was used for this model. The wall thrust contribution (ΔC_{FW}) is calculated down to the lower limit of $\dot{w}_s c_s^*/\dot{w}_p c_p^*$ for which the large-bleed theory is applicable. This corresponds to the case in which the shear layer just intersects the wall. Then, it is assumed that this wall thrust is a good approximation for the total small-bleed regime. This assumption is based on the same observation as cited previously for the constant drag assumption in the small-bleed regime. The results of these calculations are indicated in Fig. 15 by the dotted lines. The net performance curve together with the wall thrust contribution is compared with experimental data for the conical aerobell operating with air in Fig. 15a.

Carbon tetrafluoride gas was also used for some of the cold-flow testing to provide data to assist in the scaling of data to hot-firing conditions. The specific heat ratio (γ) of CF_4 varies from $\gamma = 1.17$ at sonic conditions to $\gamma = 1.31$ at $\epsilon = 27.5$ and to $\gamma = 1.35$ at $\epsilon = 55$. Thus, CF_4 undergoes "shifting" expansion caused by changes in specific heat with pressure and temperature similar to the expansion processes occurring with actual rocket engine exhaust products. However, CF_4 does have the following disadvantages when used as a rocket nozzle test medium: 1) like air, the gas tends to condense at the low pressures and temperatures resulting from expansion to high area ratios and 2) CF_4 has a relatively long "relaxation time" and cannot maintain thermodynamic equilibrium when expanded through small (scale-model) rocket nozzles because of the short stay times encountered.

Figure 15b compares the theoretical and experimental results for the conical aerobell configuration operating with CF_4 gas. Good agreement can be noted at the high secondary flow rates. However, the data falls below the theoretical curve at low secondary flow rates. The theoretical values were developed using a constant "process" or "effective" value for γ. This value was chosen as the proper exponent in the constant γ gas relationships to make the calculated value of the incremental increase in the thrust coefficient for the nozzle extension equal to the value obtained from full shifting equilibrium flow. This value was determined to be $\gamma = 1.21$.

The failure of the CF_4 to maintain equilibrium flow conditions during the expansion process appears to be the reason for the discrepancy in Fig. 15b. However, the figure does indicate the capability of the theory to analyze cases where the primary and secondary flows are different gases (CF_4 primary and air secondary). The analysis for this case was performed using the isoenergetic theory (i.e., assuming $c_s^* = c_p^*$) and then correcting for the fact that a different gas from the primary is used for the base flow by use of the c^* ratio.

The over-all thrust of the aerobell can be computed by adding the thrust of the extension to that of the basic nozzle. The over-all thrust coefficient as defined by Eq. (2) can then be obtained and compared with the experimental data shown in Fig. 4. Calculations of this type have shown that the theory can predict the over-all thrust coefficient to within 0.3%. The only exception noted was for the zero-bleed conical aerobell tested with CF_4 because of the failure of CF_4 to maintain equilibrium during the expansion. However, the accuracy for this case was still within 0.7%.

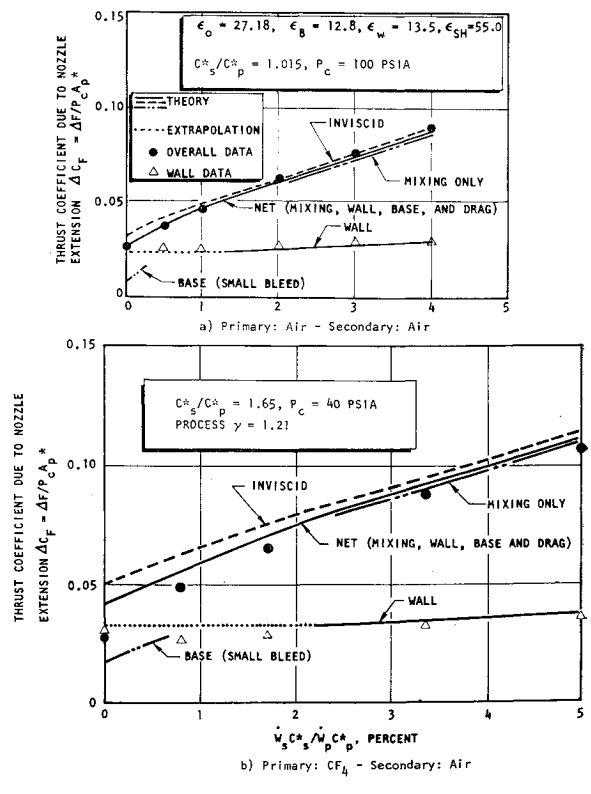

Fig. 15 Conical aerobell shroud thrust contributions.

Conclusions

The theory developed uses base flow concepts as they apply to either the small-bleed or the large-bleed regime. Experimental performance data taken from cold-flow and simulated hot-flow tests show that the theoretical model is capable of predicting both qualitatively and quantitatively the influence of the major design and operational variables. The results indicate that the use of base bleed provides good performance gains over that obtained from the basic nozzle thus indicating that the aerobell provides a method for uprating the performance of current bell nozzle thrust chambers with a minimum of development effort.

References

[1] Korst, H. H., Chow, W. L., and Zumwalt, G. W., "Research on Transonic and Supersonic Flow of a Real Fluid at Abrupt Increases in Cross Section (With Special Consideration of Base Drag Problems)," Final Report, ME-TN-392-5, Dec. 1959, Univ. of Illinois.

[2] Kirk, F. N., "An Approximate Theory of Base Pressure in Two-Dimensional Flow at Supersonic Speeds," TN Aero. 2377, March 1954, Royal Aircraft Establishment.

[3] Nash, J. F., "An Analysis of Two-Dimensional Turbulent Base Flow, Including the Effect of the Approaching Boundary Layer," Aero. Report 1036, July 1962, National Physical Lab.

[4] Addy, A. L., "On the Steady-State and Transient Operating Characteristics of Long Cylindrical Shroud Supersonic Ejectors (With Emphasis on the Viscous Interaction Between the Primary and Secondary Streams)," Ph.D. thesis, 1963, Univ. of Illinois.

[5] Korst, H. H. and Chow, W. L., "Non-Isoenergetic Turbulent ($PR_t = 1$) Jet Mixing Between Two Compressible Streams at Constant Pressure," CR-419, April 1966, NASA.

[6] Page, R. H., "The Non-Isoenergetic Turbulent Jet Mixing of a Two-Dimensional Supersonic Jet with Consideration of its Influence on the Base Pressure Problem," Ph.D. thesis, Feb. 1955, Univ. of Illinois.

DECEMBER 1969 J. SPACECRAFT VOL. 6, NO. 12

A Hazards Model for Exploding Solid-Propellant Rockets

J. C. McMunn*
TRW Systems, Redondo Beach, Calif.

AND

Jon D. Collins†
J. H. Wiggins Company Inc., Palos Verdes Estates, Calif.

AND

Billings Brown‡
Hercules Powder Company, Magna, Utah

A model is developed for predicting in a probabilistic sense the number of casualties or fatalities resulting from an exploding solid-propellant rocket. A casualty expectation equation is developed in terms of the degree of population protection, the missile impact probability in any populated area, the casualty area of the hardware and firebrand debris and the land area surrounding the impact point. The casualty area is a function of impacting propellant weight and therefore varies with flight time. These expressions are based as much as possible on data from actual flight failures and tests of both composite and double-base propellants. A numerical example is presented for a hypothetical missile; and the accuracy of the casualty expectation is estimated by computing the standard deviation. The primary use of this model is to control the planning of missile flights in order to protect people.

Introduction

SOLID-PROPELLANT rockets have propellants that are often classified as high explosives for purposes of transportation and handling. Special precautions must be taken during launch and flight to insure adequate protection to humans; among these include onboard destruct devices, flight corridors away from populated areas, and evacuation near the launch site. Sometimes a malfunctioning rocket is uncontrollable resulting in an erratic flight that breaks the rocket into several pieces; at the same time the Range Safety Officer initiates the destruct device which punctures each stage case igniting the propellant. The ignited stages explode upon ground impact producing an overpressure region and many firebrands which are thrown out to large distances. Thus, even though rocket flight is terminated, a hazard is present which is particularly acute early in flight when most of the propellant is unburned. At later flight times the main hazard is from rocket hardware. The objective of this paper is to examine the nature and the extent of the explosion from impacting solid-propellant rockets and to assess the resulting hazards. Hazards are defined only in terms of risk to human life.

In accomplishing this objective a model is developed which quantifies risk, a term which is generally treated only qualitatively. A conservative approach is taken so that computed

Presented as Paper 69-461 at the AIAA 5th Propulsion Joint Specialists Conference, U.S. Air Force Academy, Colo., June 9–13, 1969; submitted July 23, 1969, revision received September 15, 1969. The majority of this work was accomplished at TRW Systems under the sponsorship of OOAMA, USAF, Contract F42600-68-C-2325.

* Head, Structural Dynamics Section, Applied Mechanics Laboratory.

† Vice President. Member AIAA.

‡ Senior Technical Specialist, Advanced Products Engineering. Member AIAA.